Chemical Engineering of Aerogel Morphology Formed under Nonsupercritical Conditions for Thermal Insulation

B. E. Yoldas,[†] M. J. Annen,*[,‡] and J. Bostaph[§]

Formerly of the Department of Chemical Engineering, Carnegie Mellon University, Pittsburgh, Pennsylvania 15213-3890, 3M Company, 3M Center Building 208-1-01, St. Paul, Minnesota 55144-1000, and Motorola Labs, Physical Sciences Research Laboratories, 2100 East Elliot Road, Mail Drop EL508, Temple, Arizona 85284

Received June 1, 1999. Revised Manuscript Received June 12, 2000

Aerogels are among the best thermal insulating materials known. This property arises from the fact that in these materials the gaseous phase, which may occupy over 90% of the volume, is compartmentalized to a size smaller than the mean free path of air, thus severely restricting its thermal conductivity. The solid framework, which compartmentalizes the gaseous space with a minimum amount of solid, is fragile and thus must be assembled in a liquid phase that is later extracted under supercritical conditions to create the porosity. This requirement for supercritical liquid extraction, to eliminate surface tension, makes the process costly and often unsuitable for large-scale commercial applications. By computer-designed experiments, an investigation was conducted in order to produce aerogels under non-supercritical conditions. Silica aerogels having approximately 80% porosity were produced under atmospheric conditions. Moreover, the resulting pore morphology is more restrictive to thermal conductivity than that produced under supercritical conditions. This aerogel was also transformed into a micronized powder form without affecting its pore morphology, by interruption of its gelling state, thus eliminating solid-state grinding. In this paper the design of this aerogel, its pore morphology, micronization, hydrophobizing, and its use in thermal insulation are discussed.

1. Introduction

Recent restrictions on the use of chlorofluorocarbons, coupled with increasing demand for higher energy conservation, have stimulated a worldwide effort to develop a new class of thermal insulation materials. As seen from Table 1, aerogels could double or triple the thermal insulation performance of existing materials without the use of vacuum or chlorofluorocarbon gases. This unique thermal property of aerogels derives from an elegant manipulation of its pore morphology that is constituted by two phases, solid and gaseous. Various aspects of thermal conductivity through porous materials have been vigorously treated in other papers.[1−7] Here it suffices to introduce the concept in its simplest form to elucidate the effect of pore morphology on thermal conductivity.

Table 1. Thermal Conductivity of Various Materials

materials	thermal conductivity (W/(m K))	*R*-factor
air	0.025	5.7
CCl_2F_2	0.012	11.6
CCl_3F	0.007	20
dense polyurethane	0.15	1.0
polyurethane foam	0.04	3.5
polyurethane foam with CFC	0.021	7.0
dense silica glass	1.00	0.1
silica powder	0.025	6
silica powder (evacuated)	0.004	35
silica aerogel	0.008	11
silica aerogel (evacuated)	0.002	70−100

The total heat transfer through a porous material (λ'_t) is the sum of the heat transfer through solid phase (λ'_s) and gas phase (λ'_g) and by radiation (λ'_r).

$$\lambda'_t = \lambda'_s + \lambda'_g + \lambda'_r + \text{coupling terms} \qquad (1)$$

Heat transfer through the gas phase is composed of conduction since aerogel pore sizes are too small for convection. The thermal conduction by radiation λ'_r is also relatively small[1−6] in most applications and can be ignored[2−5] for the purpose of this discussion. Thus, we will only be concerned with the sum of the conductive heat transfer through the two phases that make up the structure, namely, $\lambda'_s + \lambda'_g$.

[†] Formerly of the Carnegie Mellon University.
[‡] 3M Company.
[§] Motorola Labs.
* To whom correspondence should be addressed.

(1) Kaviany, M. *Principles of Heat Transfer in Porous Media;* Springer-Verlag: New York, 1991.
(2) Fricke, J.; Lu, X.; Wang, P.; Buttner, D.; Heinemann, U. *Science* **1992**, *255*, 2308.
(3) Hrubesh, L. W.; Pekala, R. W. *J. Mater. Res.* **1994**, *9*, 731.
(4) Rettelbach, Th.; Sauberlich, J.; Korder, S.; Fricke. J *J. Non-Cryst. Solids* **1995**, *186*, 278.
(5) Fricke, J. *Sci. Am.* **1988**, *258* (5), 92.
(6) Brinker, J. C.; Keefer, K. D.; Schaefer D. W.; Ashley, C. S. *J. Non-Cryst. Solids* **1982**, *48*, 47.
(7) Gross, J.; Fricke, J. *J. Non-Cryst. Solids* **1992**, *145*, 217.

10.1021/cm9903428 CCC: $19.00
Published on Web 07/29/2000

Fricke et al.[2] and Hrubesh et al.[3] show that the heat transfer λ'_s through the solid phase in aerogels is given by

$$\lambda'_s = \lambda^\circ_s V_s (v_p/v_d) \tag{2}$$

λ°_s is the intrinsic conductivity of the solid that makes up the aerogel (i.e., SiO_2), v_p/v_d is the ratio of the sound velocities in porous and dense bodies, V_s is the volume fraction of the solid, and V_g is the volume fraction of the voids or fractional porosity $= (1 - V_s)$. According to eq 2, the solid-phase thermal conductivity can be directly lowered through a reduction in the solid volume fraction, V_s. This reduction must be compensated by a corresponding increase in the gaseous volume, since $V_s + V_g = 1$, which would normally result in an increase in the gas-phase heat transfer. However, the thermal conductivity of the gas phase can also be dramatically reduced without altering its volume fraction, by compartmentalizing the gaseous phase into domains (pores) smaller than the mean free path of the gas molecules. This pore size dependency of the gaseous thermal conductivity is evident from the following equation:[1,2,3,8]

$$\lambda'_g = \lambda^\circ_g V_g/(1 + \beta K_n) \tag{3}$$

where β is a gas constant and K_n is the dimensionless Knudsen number defined[9] as $K_n = l/d$, where l is the mean free path of the gas molecules and d is the pore diameter. For air under ambient conditions, these numbers are approximately[1−3] $\lambda^\circ_g = 2.534 \times 10^{-2}$ W/(m K), $\beta \approx 2$, and $K_n \cong 70/d$, where d is the diameter in nanometers. Thus eq 3 becomes

$$\lambda'_g = \frac{2.534 \times 10^{-2} V_g}{1 + 140/d} \tag{4}$$

with λ in W/(m K) and d in units of nanometers.

For $d \gg 140$ nm, the gaseous conductivity depends only on the total porosity:

$$\lambda'_g \approx 2.5 \times 10^{-2} V_g \qquad \text{for } d \gg 140 \text{ nm} \tag{5}$$

When the pore size d is extremely small, i.e., $d \ll 140$ nm, eq 4 can be reduced to

$$\lambda'_g \approx 1.7 \times 10^{-5} V_g d \qquad \text{for } d \ll 140 \text{ nm} \tag{6}$$

As seen from eq 5, when d is large, e.g., micron range, the gaseous conductivity in porous materials is directly proportional only to the porosity V_g. When d is small (<100 nm), the gaseous conductivity becomes a function of both the porosity and the pore size, as seen from eq 6.

In those cases where pore sizes are below the mean free path of air molecules, reducing either the porosity or the pore size reduces the thermal conductivity of the gaseous phase. The important observation is that the reduction of porosity can only occur by a corresponding increase in solid volume, which contributes to the overall thermal conduction. On the other hand, a reduction in thermal conductivity achieved by reducing the pore size, without reducing total pore volume, does not have a penalty. Thus, the most effective way to reduce the total thermal conduction is to first reduce the solid thermal conductivity by increasing the porosity and then reduce the gaseous phase conductivity by reducing the pore size below the mean free path of air. However, combining high porosity and small pore size in the same material becomes an extremely difficult task. The reason for this is, while the fracture strength of materials decreases exponentially with porosity,[10] dropping nearly 2 orders of magnitude at 80%−90% porosity, the capillary pressure exerted on the structure during liquid extraction increases with decreasing pore size:[11,12]

$$p = -\frac{2\gamma \cos(\theta)}{r} \tag{7}$$

where p is the capillary pressure, γ is the surface tension, r is the pore radius, and θ is the wetting angle. As a result, under normal drying conditions the fragile aerogel structure collapses. However, as evident from eq 7, the capillary pressure can be abated by mediation of the surface tension or the wetting angle of the liquid. These avenues have been investigated extensively.[13,14]

One apparent way of eliminating the capillary force altogether is to reduce the surface tension to zero under supercritical conditions. Kistler in 1932 produced silica aerogels in autoclaves by this method.[15] Since then, aerogel formation has been intensively investigated.[16−22] Supercritical conditions require processing under high temperatures (T_c) and pressures (P_c) for most common solvents, e.g., 374 °C and 3204 psi for water and 240 °C and 1155 psi for methanol. Hurt et al. developed a process in which alcohol is replaced by liquid CO_2 during the liquid extraction, thus reducing the explosion concerns as well as reducing the supercritical temperature significantly ($T_c = 31$ °C, $P_c = 939$ psi).[23−26] Nevertheless, the requirement for high-pressure supercritical liquid extraction is a significant barrier for mass production of aerogels.[27−31]

(8) Lu, X.; Aronini-Schuster, M. C.; Kuhn, J.; Nilson, O.; Fricke, J.; Pekala, R. W. *Science* **1992**, *255*, 274.
(9) Cussler, E. L. *Diffusion;* Cambridge University Press: New York, 1984; p 187.
(10) Kingery, W. D. *Introduction to Ceramics*; John Wiley & Sons: New York, 1960; pp 621−622.
(11) Dullien, F. A. L. *Porous Media, Fluid Transport and Pore Structure*; Academic Press: New York, 1979.
(12) Scherer, G. W. *J. Non-Cryst. Solids* **1989**, *109*, 171.
(13) Smith, D. M.; Deshpande, R.; Brinker, J. C. *Mater. Res. Soc. Symp. Proc.* **1994**, *271*, 567.
(14) Smith, D. M.; Stein, D.; Anderson, J. M.; Ackerman, W. *J. Non-Cryst. Solids* **1995**, *186*, 104.
(15) Kistler, S. S. *Nature* **1931**, *127*, 741.
(16) Schaefer, D. W.; Keefer, K. D. *Phys. Rev. Lett.* **1986**, *56*, 2199.
(17) Iler, R. *The Chemistry of Silica*; J. Wiley and Sons: New York, 1979.
(18) Schaefer, D. W.; Wilcoxon, J. P.; Keefer, K. D.; Bunder, B. C.; Pearson, R. K.; Thomas, I. M.; Miller, D. E. *Physics and Chemistry of Porous Media II;* AIP Conf. Proc. Vol. 154; Banavar, J. R., Koplik, J., Winkler, K. W., Eds.; American Institute of Physics: New York, 1987; p 63.
(19) Schaefer, D. W. *J. Phys., Colloq.* **1998**, *4*, C4−121.
(20) Schaefer, D. W. *Science* **1989**, *243*, 1023.
(21) Brinker, C. J.; Scherer, G. W. *Sol−Gel Science*; Academic Press: New York, 1990; Chapter 3.
(22) Hrubesh, L. W.; Tillotson, T. M.; Poco, J. F. In *Chemical Processing of Advanced Materials*; Hench, L. L., West, J. K., Eds.; J. Wiley and Sons: New York, 1992; p 19.
(23) Tewari, P. H.; Hurt, A. J. US Patent 4,610,863, 1986.
(24) Tewari, P. H.; Hurt, A. J.; Lofftus, K. D. *J. Mater. Lett.* **1985**, *3*, 363.
(25) van Bommel, M. J.; de Haan, A. B. *J. Mater. Sci.* **1994**, *29*, 943.
(26) Tillotson, T. M.; Hrubesh, L. W. *J. Non-Cryst. Solids* **1992**, *145*, 44.

Now let us look at the chemical process that leads to aerogel formation itself. The reactions leading to silica network formation from silicon alkoxides, $Si(OR)_4$, can be represented as

hydrolysis:

$$(OR)_3Si-OR + HOH \rightarrow (OR)_3Si-OH + R(OH) \quad (8)$$

followed by

polymerization:

$$(OR)_3Si-OH + RO-Si(OR)_3 \rightarrow \equiv Si-O-Si\equiv + R(OH) \quad (9)$$

The overall hydrolytic polycondensation reaction can be represented as

$$nSi(OR)_4 + mH_2O \rightarrow Si_nO_{2n-(x+y)/2}(OH)_x(OR)_y + (4n - y)R(OH) \quad (10)$$

Note that hydrolytic polycondensation of the alkoxide can never result in the formation of pure oxides due to the presence of terminal groups.[32−34] Since $Si(OR)_4$ and H_2O are not miscible, the reaction is normally carried in a mutually miscible solvent such as alcohol and requires a catalyst. Acid catalysts commonly produce tight networks whereas basic catalysts can give more open networks leading to true aerogel formation.[21] The role of water during hydrolytic condensation goes far beyond its participation in the chemical reaction. Dilution of the reaction medium by solvent affects not only the surface tension and contact angle but also statistical interactions of reacting species; thus, it becomes one of the significant process parameters that determines the molecular size and polymer morphology.

Our primary objective in this work was to determine the technical feasibility of producing highly porous silica aerogels by manipulation of processing parameters, that is, by means other than supercritical drying. Our secondary objective was to determine the viability of using these materials in low-cost thermal insulation systems in the following configurations: (i) large aerogel monoliths, (ii) powder in pouches, and (iii) composites with organic polymers.

2. Experimental Section

The main processing parameters in the formation of silica aerogels from silicon alkoxide are first identified as (i) precursor of alkoxide, e.g., $Si(OCH_3)_4$ or $Si(OC_2H_5)_4$; (ii) water/alkoxide ratio; (iii) type of solvent, e.g., type of alcohol; (iv) type and concentration of catalyst; (v) molecular spacing, i.e., concentration of alkoxide in the solvent; (vi) temperature; and (vii) presence of surfactants. The general effects of these parameters on pore morphology were first individually determined by keeping all other parameters constant.

For this work, silicon tetramethoxide and silicon tetraethoxide were purchased from United Chemical Technologies, Inc. (Bristol, PA); all other reagents were purchased from Aldrich Chemical Co. (Milwaukee, WI).

Initially, silicon tetramethoxide, $Si(OCH_3)_4$, and NH_4OH were chosen as the silica precursor and catalyst, respectively, for kinetic reasons. Samples were prepared by first mixing water, solvent, and catalyst in a glass container and adding to this mix the $Si(OCH_3)_4$. After mixing, the container was sealed and kept at 50 °C for 24 h. In most cases the gelling occurred within the first hour. The viscosity change during the gelling period was also measured by a Hercules viscometer in selected samples. After 24 h the containers were unsealed, and the samples were allowed to partially dry at 50 °C and then heated to 100 °C for further drying.

Approximately 200 nitrogen adsorption and desorption isotherms were collected at 77 K on a Micromeritics ASAP 2000 gas sorptometer. The BET[35] model was used for calculation of surface area (SA), and pore size distributions were calculated from the desorption isotherm using the BJH[36] model. The isotherms were all characterized as type IV,[37] with the total pore volume (V_{pore}) calculated from the highest partial-pressure adsorption point. The average pore diameter (d_p) was then calculated using the equation $d_p = 4V_{pore}/SA$. For calculations of porosity, a nonporous silica density of 2.2 g/cm^3 was used.

The relative degree of hydrophobicity of surface-modified aerogels was measured by rigorously agitating slurries of the aerogel powder in methanol/water solution. Results are reported as the maximum weight percent methanol in water in which the aerogel floated.

Early in the experimentation it became apparent that the three most influential condensation parameters were the water/alkoxide ratio, concentration of ammonia, and solvent type/concentration. We then designed statistical experiments to establish the effects of condensation parameters on pore morphology using statistical experimental design.

After establishing the optimum conditions for silica aerogel formation under non-supercritical conditions, we also investigated the hydrophobization of their surfaces as well as the feasibility of using micronized aerogel powders as insulation materials both by themselves and in combination with paint and polyurethane foam.

Initially, powders were produced by mechanical micronization of the monolithic aerogels after drying. Later it was discovered that powders with a similar particle size distribution could be obtained by subjecting these sols to high shear during the gelling process, using common household blenders stirring at 2000−3000 rpm. This not only eliminated a costly and time-consuming mechanical pulverization process but also significantly accelerated drying of the aerogels.

Because of the toxicity of the methanol byproduct of the polycondensation of $Si(OCH_3)_4$, the use of $Si(OC_2H_5)_4$ as the aerogel precursor was also investigated since the ethanol byproduct is less hazardous. In some applications it was necessary to hydrophobize these aerogels to protect their integrity against moisture and water. These experiments were conducted by chemically creating surface hydroxyl groups and subsequently reacting them with the vapor of alkylalkoxysilanes or chloroalkoxysilanes.

Thermal conductivity tests of aerogel powders were conducted at Oak Ridge National Laboratories (ORNL) under varying atmospheric pressures in sealed pouches. In another set of experiments, aerogel powders were blended with paint and incorporated into polyurethane foam; their properties were investigated at the Detroit Polymer Institute.

(27) van Bommel, M. J.; de Haan, A. B. *J. Non-Cryst. Solids* **1995**, *186*, 78.
(28) Schwertfeger, F.; Husing, N.; Schubert, U. *J. Sol-Gel. Sci. Technol.* **1994**, *2*, 103.
(29) Carlson, G.; Lewis, D.; McKinley, K.; Richardson, J.; Tellotson, T. *J. Non-Cryst. Solids* **1995**, *186*, 372.
(30) Schwertfeger, F.; Frank, D.; Schmit, M. *J. Non-Cryst. Solids* **1998**, *225*, 24.
(31) Smith, D. M.; Stein, D.; Anderson, J. M.; Ackerman, W. *J. Non-Cryst. Solids* **1995**, *186*, 104.
(32) Yoldas, B. E. *J. Am. Ceram. Soc.* **1982**, *65*, 387.
(33) Yoldas, B. E. *J. Non-Cryst. Solids* **1982**, *51*, 105.
(34) Yoldas, B. E. *J. Polym. Sci., Part A: Polym. Chem.* **1986**, *24*, 3475.
(35) Gregg, S. J.; Sing, K. S. W. *Adsorption, Surface Area and Porosity*; Academic Press: New York, 1982.
(36) Barrett, E. P.; Joyner, L. G.; Halenda, P. P. *J. Am. Chem. Soc.* **1951**, *73*, 373.
(37) Brunauer, S.; Deming, L. S.; Deming, W. S.; Teller, E. *J. Am. Chem. Soc.* **1940**, *62*, 1723.

Table 2. Effect of Selective Processing Parameters on the Pore Morphology of Silica Network Condensed from $Si(OCH_3)_4$

I. Alcohol Effect[a]

alcohol	av pore diameter (Å)	pore vol (cm^3/g)	porosity (%)	surface area (m^2/g)
methanol	52	1.19	72	865
ethanol	54	1.20	73	844
2-propanol	118	1.52	77	532

II. $Si(OCH_3)_4$ Concentration Effect[b]

$Si(OCH_3)_4$ concn (wt %)	av pore diameter (Å)	pore vol (cm^3/g)	porosity (%)	surface area (m^2/g)
10	92	1.46	76	627
20	118	1.60	78	532
40	105	1.63	78	609

III. NH_4OH Concentration Effect[c]

NH_4OH (g)	av pore diameter (Å)	pore vol (cm^3/g)	porosity (%)	surface area (m^2/g)
0.02	100	1.54	77	608
0.15	84	1.35	75	635

[a] One mole $Si(OCH_3)_4$ condensed with 2 mol of H_2O and 0.02 g of NH_4OH in 480 g of these alcohols. [b] One mole $Si(OCH_3)_4$ condensed with 2 mol of H_2O and 0.01 g of NH_4OH in 2-propanol at these concentrations. [c] One mole of $Si(OCH_3)_4$ condensed with 2 mol of H_2O in 480 g of 2-propanol under these concentrations of ammonia.

Table 3. Aerogel Pore Morphology Resulting from Solvent Effect on $Si(OCH_3)_4$

solvent	porosity (%)	pore diam (Å)	size distribution (Å)
2-propanol	80.0	88.0	50−110
1-propanol	75.8	85.2	80−120
sec-butanol	76.4	127.2	100−320
1-butanol	74.5	102.0	80−220
ethanol	72.0	54.4	
methanol	74.5	63.0	50−100
acetone	75.7	134.3	100−200
methyl ethyl ketone	55.6	85.6	80−310
diacetone	73.6	95.9	80−120
tetrahydrofuran	63.7	87.7	80−230
ethylene glycol monomethyl ether	70.4	68.3	65−100, 300−400
tributylamine	74.0	74.5	80−110

3. Results and Discussion

3.1. Pore Morphology Development. Table 2 shows the effects of select processing parameters on pore size, pore volume, and surface area of silica networks condensed from $Si(OCH_3)_4$, as determined by nitrogen absorption−desorption isotherms. Table 3 shows the percent porosity of silica aerogels obtained by hydrolytic polycondensation of 1 mol of $Si(OCH_3)_4$ with 2 mol of H_2O and 0.02 g of NH_4OH in 500 g of various solvents. The results consistently show that hydrolytic polycondensation of $Si(OCH_3)_4$ in propyl alcohols yields the highest porosity in the resultant silica aerogel. Then, using isopropyl alcohol as the hydrolysis medium, experiments were designed to determine the maximum porosity that can be attained in silica aerogels under non-supercritical conditions and the corresponding pore morphology.

Figure 1 shows a computer-generated topological map of porosity in the fields of water and alcohol concentration (given as grams per mole of $Si(OCH_3)_4$ in this figure). These topological maps were generated by ECHIP software[38] using BET results of approximately

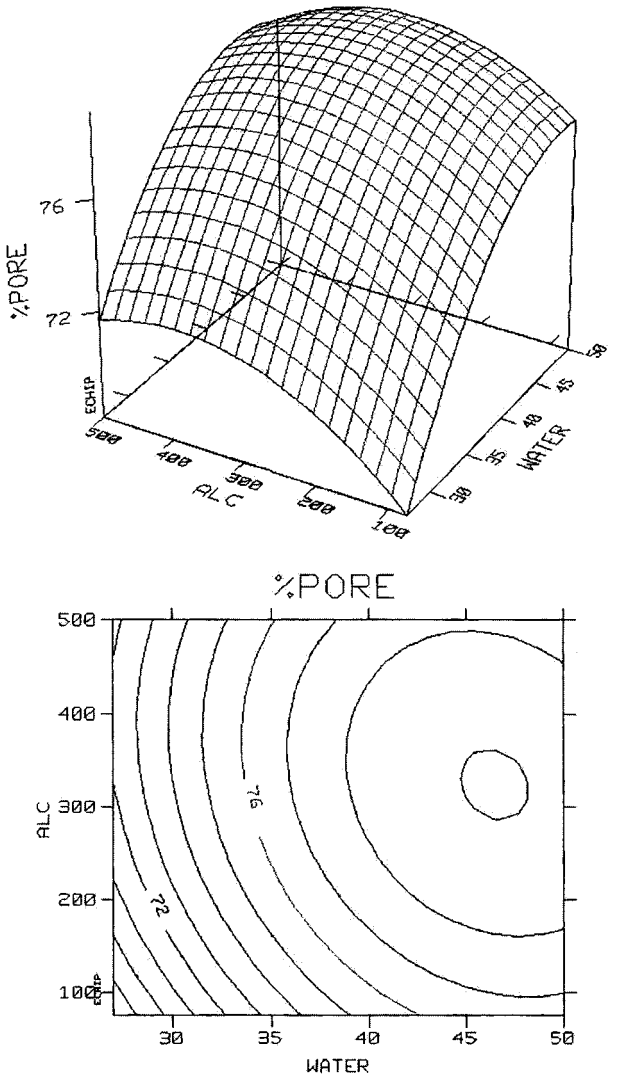

Figure 1. Computer-generated topological map of porosity in the field of water and propyl alcohol concentration (given as gram weight per mole of $Si(OCH_3)_4$).

200 samples. The accuracy of the map was checked with numerous additional data points. The bottom figure shows the porosity contour lines in two-dimensional space, indicating the precise location of the maximum porosity that can be attained in this field. This maximum porosity, 79−80%, occurs when ∼47 g of H_2O (∼2.6 mol) and 330 g of C_3H_7OH (5.5 mol) are used per mole of $Si(OC_3H_7)_4$ along with 300 mg of NH_4OH. Since pore volume by itself would not be meaningful in thermal conductivity applications without a related pore size and pore size distribution, information on similar topological maps for the pore size was also obtained. Figure 2 shows the mean pore size contours in the same water−alcohol field when $Si(OCH_3)_4$ is condensed with 300 mg of NH_4OH catalyst per mole. Figure 3 shows the pore size distribution curve of ∼80% porous, non-supercritically produced silica aerogel as established by the nitrogen desorption isotherms. In contrast, the pore size distribution curves of supercritically produced silica aerogels THERMALUX and our N_2 sorption measurements of BASF aerogel powder indicate a much wider size distribution between 100 and 500 Å.

(38) ECHIP, Inc., Hockessin, DE 19707.

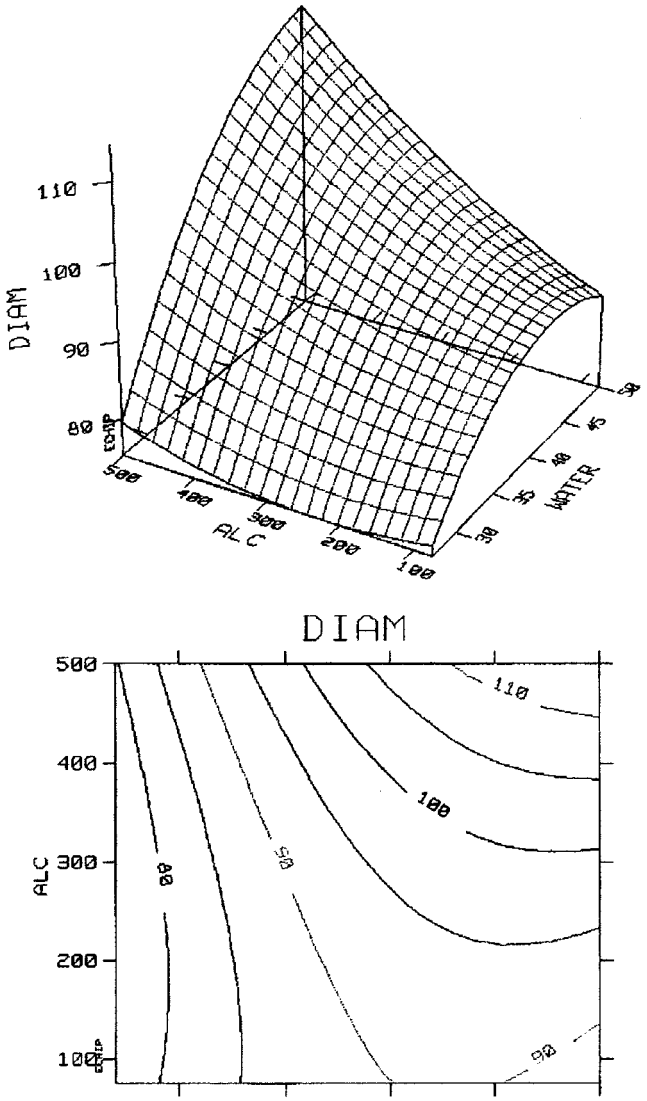

Figure 2. Mean pore size contours in the water−propanol field.

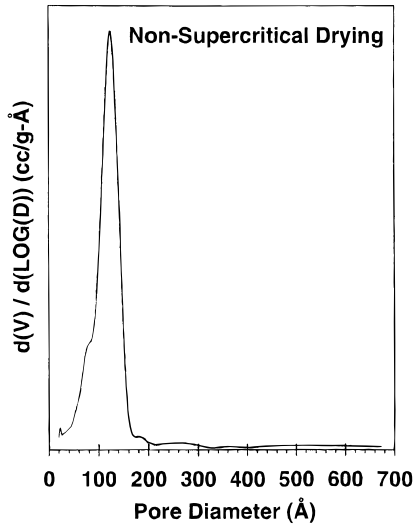

Figure 3. Pore size distribution of 80% porous, non-supercritically produced silica aerogel.

The comparison of thermal insulation performance between these two systems is rather complex. The aerogels produced under supercritical conditions have higher (~93%) porosity. THERMALUX is produced as monolithic panels as large as 12 in. × 12 in. × $^1/_2$ in. in autoclaves in several steps. The solvent (alcohol) is exchanged with liquid CO_2 to lower the critical temperature from ~240 to 31 °C, but the critical pressure must remain high. BASF aerogel is also produced under supercritical conditions; however, it is produced as a powder using a spraying technique.

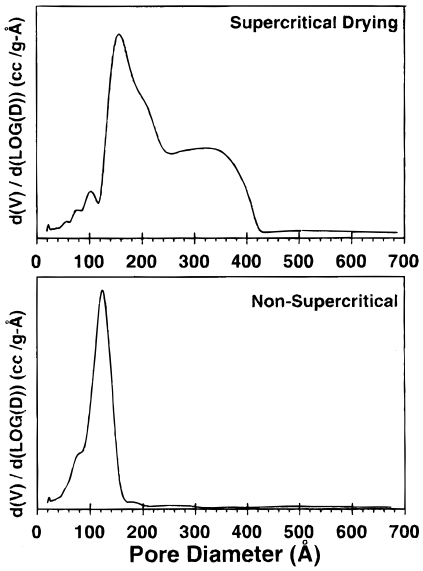

Figure 4. Comparison of pore size distribution of supercritically produced THERMALUX and non-supercritically produced silica aerogel.

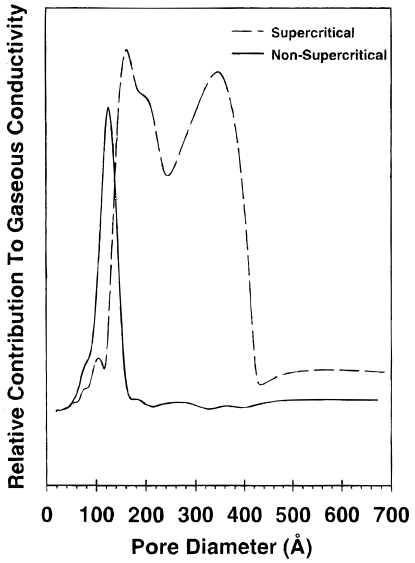

Figure 5. Effect of pore size distributions of THERMALUX and the non-supercritically produced silica aerogel on the relative contribution to gaseous thermal conductivity.

Figure 4 compares the relative pore size distributions between supercritically produced THERMALUX and nonsupercritically produced silica aerogel in this investigation. Figure 5 shows their relative contributions to thermal conductivity. Figure 6 displays computer-generated curves[2,3] showing how the pore size below the mean free path affects the thermal conductivity. As seen in that figure, the effect of pore size on thermal conductivity is optimized around 94% porosity in silicas. At this porosity, reducing the pore size from 100 to 10 nm would represent a reduction in thermal conductivity

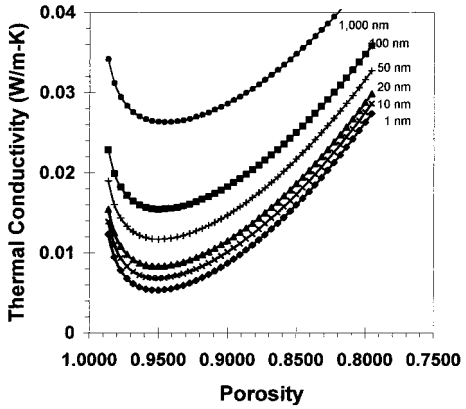

Figure 6. Pore size effect on overall thermal conductivity of SiO_2 aerogels at 300 K in air.

by a factor of 3 (from 0.0154 to 0.0053 W m^{-1} K^{-1}). However, with such small pore size it is virtually impossible to attain such high porosities (due to inversely related capillary forces). Nevertheless, at this porosity an achievable reduction of the pore size from ~50 to ~10 nm represents a total thermal conductivity reduction of ~42%. In less porous systems, as expected, the pore size effect becomes somewhat less but remains significant. At the 80% porosity level of the non-supercritically produced silica aerogels, a pore size change from ~50 to ~10 nm represents a thermal conductivity reduction of 13% from 0.0316 to 0.0275 W m^{-1} K^{-1}.

The *R*-factor topology is shown in Figure 7, where $R = L/\lambda'_t$ in units of (h ft^2 °F)/Btu [0.145 W/(m K) = Btu in./(h ft^2 °F), *L* is the insulator thickness which is normalized to 1 in. in this work, and λ'_t is the overall thermal conductivity]. The data in Figure 7 indicate that a maximum *R*-factor of 14 occurs slightly offset from where the maximum porosity occurs in the same hydrolytic condensation field in this material. This *R*-factor of 14 is approximately twice as high as the polyurethane *R*-factor with CFC gases and higher than that of supercritically produced THERMALUX with $R = 11$.

3.2. Micronization in Gel State. We were unable to produce large crack-free aerogel panels under non-supercritical conditions. Aerogel granules 1−3 in. in size were produced and could not be used as a thermal insulation material in this form due to the large intergranular spaces. However, the micronized form of this material (particle size distribution shown in Figure 8) can be sealed in pouches, thereby eliminating gaseous conductivity entirely while providing physical containment of the powder in a desired shape and flexibility. This particle size distribution is very similar to that of any micronized precipitated silicas and appears to be directly related to the micronization and particle collection processes.

We have attempted to explore the possibility of producing fine-powder aerogel by interfering with the gelling dynamics in the liquid state because micronization of solid matter is tedious, time-consuming, and costly. Experiments indicated that gelation under vigorous stirring restricted structural connectivity to small domains that dried to fine aerogel particles, depending on the degree of agitation. Gelling the precursor sol in household blenders at several thousand rpm produced a gel aggregate, which, when dried, yielded aerogel

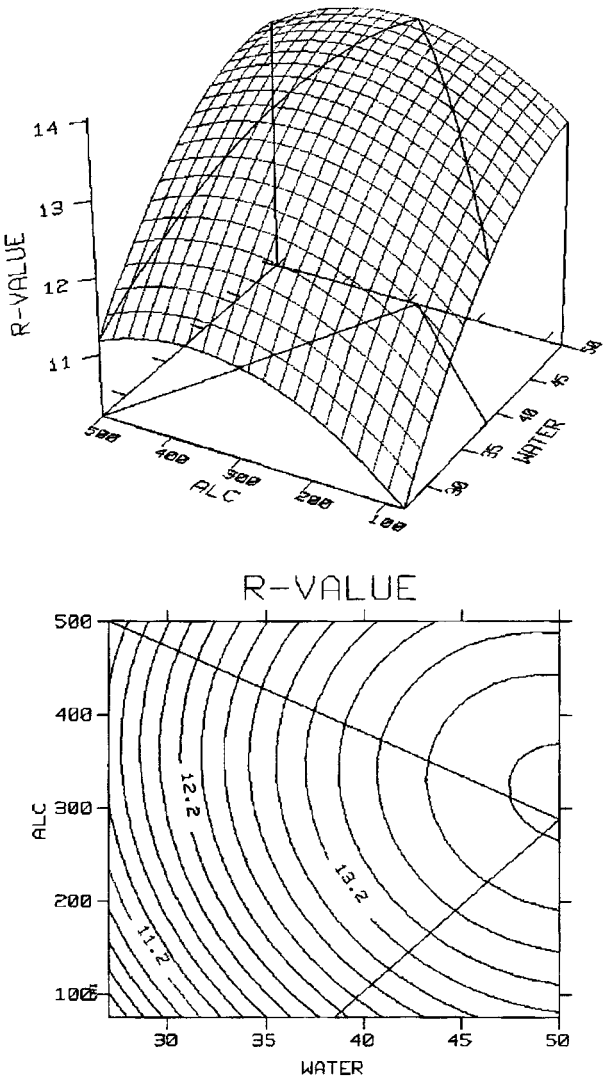

Figure 7. *R*-factor topology in the water−propanol field.

powder whose particle size and size distribution was very similar to that of the micronized aerogel shown in Figure 8.

Figure 9 shows the dynamics of the gelation of the aerogel precursor and its microfracture as measured by a Hercules viscometer at 2800 rpm. As seen during the initial 400 s (6.5 min) after the solution is mixed, its viscosity remains flat at around 2.5 cP. This is followed by a dramatic increase in the viscosity from 2.5 to ~40 cP during the following 300 s. At this point (~11−12 min into the process), the gel's structure is sufficiently solidified and starts to microfracture with further agitation; thus, the viscosity falls. The whole process, i.e., from gelation to micronization, is completed within 20 min. Such a microfractured gel powder can be rapidly air-dried to a fine powder. It was also observed that this interruption of the gelling state does not appear to affect the internal pore morphology and fundamental ultrastructure. Thus, the micron-sized particles are still 80% porous, and the pore size and size distribution under dynamic gelling are similar to that shown in Figure 3.

3.3. Thermal Insulation by Aerogel Powder. Figure 10 displays insulation "*R*" values of powder packs of aerogel powder, precipitated silica, and a typical commercial silica, as a function of gaseous pressure under constant volume. In this measurement performed

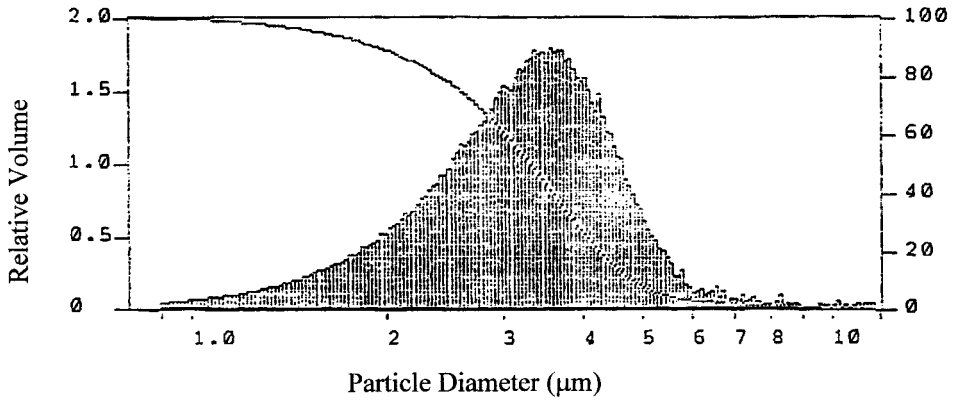

Figure 8. Particle size distribution of micronized aerogel.

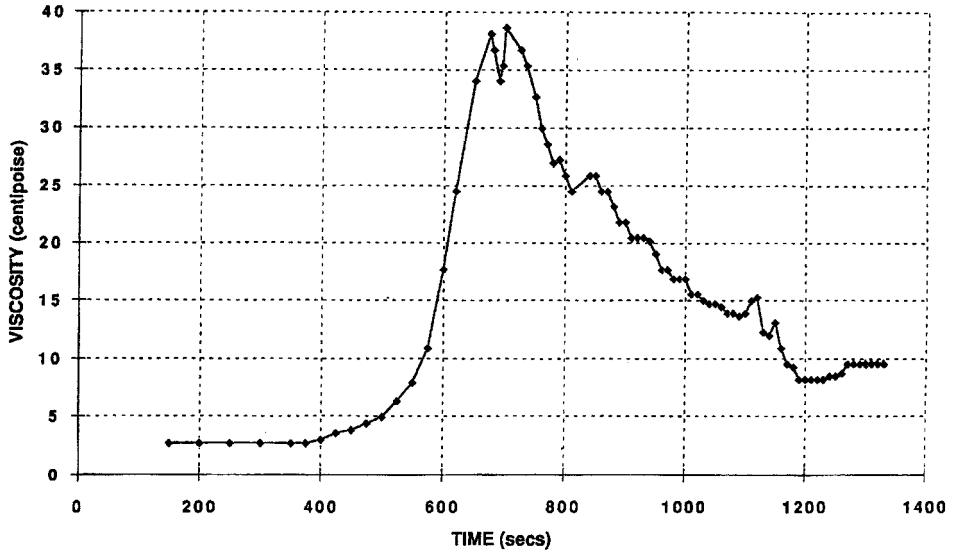

Figure 9. Viscosity change of aerogel precursor sol as a function of time when gelled under dynamic stirring at 2800 rpm.

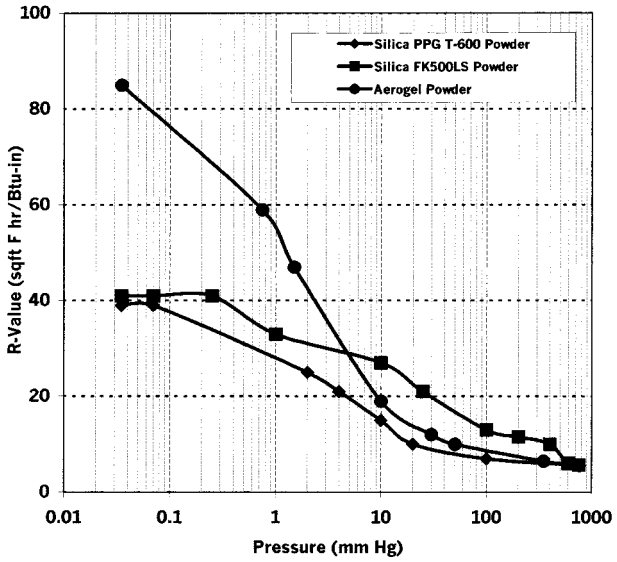

Figure 10. Constant-volume "*R*" value comparisons of various silica powder packs at different evacuation pressures.

at ORNL, the powders are packed in a metal cylindrical chamber, and the chamber is evacuated. *No powder compaction occurs*; i.e., the system stays ~90% porous. As the pressure approaches standard atmospheric pressure, *R* values approach that of air, i.e., ~6 h ft^2 °F/Btu in all cases. This means that a significant portion of the porosity in these powder packs is due to pores whose sizes are larger than the mean free path of air (which is also clearly indicated by the electron micrographs). Thus, the measurements reflect the dominating gaseous conductivity of the interparticle space.

Table 4. Effect of Micronization on Density, Porosity, and Type of Porosity

material	density (%)	total porosity (Å)	internal[a] porosity	interparticle[b] porosity
aerogel monoliths	0.45	80%	80%	
micronized aerogel	0.12	95%	20%	75%
precipitated silica (PPG T-700)	0.06	97%		97%

[a] Chemical created internal porosity, 50−100 Å. [b] Physically produced coarse aggregate porosity.

Table 4 summarizes densities and porosities of aerogels before and after micronization. The striking feature of the data is that, before the micronization, 80% of the existing porosity is internal. After micronizing a large portion of the total porosity is external to the particles, i.e., 75%. Thus, when the powder packs are extremely porous (e.g., 90%), air freely conducts through these large interparticle pores and dominates the overall conductivity (corresponding to $R = 5.7$ for air), unless they are evacuated. A more noteworthy feature of these measurements indicated in Figure 10 is that a distinct difference starts to occur between aerogel silicas and precipitated silicas as the pressure diminishes toward

Table 5. Effect of Micronized Silica Aerogel in Paint

sample	thermal conductivity (W/(m K))	*R* value
glass[a]	0.870	0.166
glass + paint	0.854	0.169
glass + paint w/6% aerogel	0.559	0.258

[a] $^1/_8$ in. soda lime float glass.

vacuum. At these low pressures where the solid conductivity dominates, we note that the solid conductivity of aerogel structures is only about one-half that of precipitated silicas for the same solid volume fraction. It is reasonable to assume that this arises due to the differences in particle morphology and in point contact in aerogel structures, where the fundamental particles are spherical. Thus, aerogel powders in a vacuum applications, e.g., in space, would provide substantially superior thermal insulation in comparison to precipitated silicas and other materials whose fundamental particle morphology is other than spherical.

Table 5 shows the effect of adding 6 wt % aerogel powder into a household paint. The paints, with and without aerogel, were applied on a $^1/_8$ in. thick glass surface at the same thickness. The thermal conductivity of these samples was measured by Holometrix Corp., MA. These measurements demonstrate that paint by itself provides 2 wt % improvement over the insulation of unpainted glass, whereas paint containing 6 wt % micronized aerogel shows a 35% improvement over the insulation of unpainted glass. This suggests aerogel-loaded specialty paints for insulation of hot or cold metallic surfaces such as refrigerators or motors may be of commercial interest. Another potential application is the introduction of aerogel powders into polyurethane foam. Studies at the Polymer Institute at the University of Detroit have shown that the addition as little as 1 wt % or less aerogel into polyurethane foam improved its thermal insulation as much as 10−12%. Aerogel additive in polyurethane foam is found to act as a nucleating agent promoting a finer texture with higher closed cell content, in addition to interrupting solid conductivity through the cell walls. This concept is pursued separately.

3.4. Hydrophobization of Silica Aerogels. When silica aerogels are formed by hydrolitic polycondensation of alkoxysilanes, the network structure requires the presence of terminal groups. Thus, the chemical composition corresponds to the general formula

$$Si_nO_{2n-(x+y)/2}(OH)_x(OR)_y \qquad (11)$$

The concentration of terminal groups depends strongly on the condensation conditions, particularly on the water/alkoxide ratio. The resultant aerogel is chemically unstable since its alkoxy groups, (OR), are subject to further hydrolysis by exposure either to humidity or to liquid water. Any attempt to reduce the concentration of OR terminal groups by using higher water/alkoxide ratio during the condensation results in a dramatic reduction of porosity and thus cannot be utilized. Under the condensation conditions that are designed to give optimum pore morphology for thermal insulation, the chemical composition of the resultant aerogel corresponds approximately to $Si_{10}O_{18}(OH)_1(OR)_3$. In addition to chemical instability, extremely small pore size, e.g., 10 nm, leads to condensation of water in the pores leading to collapse of the fragile structure by capillary forces. For this reason even the supercritically produced aerogel panels are normally sealed in a pouch to protect them from ambient humidity. Alternatively, the aerogel surface could be rendered hydrophobic.

Inducing hydrophobicity on silica surfaces by a vapor phase treatment is well-known and practiced commercially. In this method, silica surfaces are typically exposed to vapor phase alkylchlorosilanes, e.g., SiR_3Cl, or alkylalkoxysilanes, e.g., $SiR_3(OR^1)$, at temperatures 50−100 °C. Chlorine or alkoxy groups react with hydroxy groups of silicas, resulting in silica-bonded alkyl surface groups that are hydrophobic:

$$\equiv Si-OH + Cl-Si\equiv R_3 \rightarrow \equiv Si-O-Si\equiv R_3 + HCl \qquad (12)$$

$$\equiv Si-OH + RO-Si\equiv R_3 \rightarrow \equiv Si-O-Si\equiv R_3 + ROH \qquad (13)$$

The first reaction has the disadvantage of releasing environmentally objectionable hydrochloric acid, and the second requires a catalyst. However, either reaction converts only the "OH" terminal bonds to hydrophobic bonds. Alkoxy bonds in the aerogel, i.e.,

$$Si_nO_{2n-(x+y)/2}(OH)_x(OR)_y \qquad (14)$$

remain unreacted. For full hydrophobization, alkoxy bonds must first be converted to hydroxyl bonds by a water vapor treatment of the aerogel:

$$Si_nO_{2n-(x+y)/2}(OH)_x(OR)_y - (y/2)H_2O(\text{vapor}) \xrightarrow{T>100\ ^\circ C} Si_nO_{2n-z/2}(OH)_z + yR(OH) \qquad (15)$$

where $z = x + y$. Then fully hydrolyzed, OR-free aerogel is subjected to vapor treatment of the hydrophobizing agent, e.g., $Si(CH_3)(OCH_3)$:

$$Si_nO_{2n-z/2}(OH)_z + 2Si(CH_3)(OCH_3) \xrightarrow{50-100\ ^\circ C} Si_{n+2}O_{2n+z/2}R_{3z} + 2CH_3OH \qquad (16)$$

In these reactions a trace amount of ammonia or acid vapor can be used as a catalyst. Table 6 shows the overall changes occurring in the aerogel composition and weight during these processes.

A number of chloroalkoxysilanes and alkylalkoxysilanes were evaluated for their ability to induce hydrophobicity. For best results, it was found that both the alkyl and alkoxy groups in these compounds should be as small as possible, i.e., CH_3 and OCH_3. Therefore, the best hydrophobizing agents are $SiCl(CH)_3$, $SiCl(CH_3)_2(OCH_3)$, and $Si(CH_3)_3(OCH_3)$. The latter may be preferred since it does not produce an HCl byproduct. The most hydrophobic aerogels were produced by a simple exposure of the fully hydrolyzed materials to $SiCl(CH_3)_2(OCH_3)$ vapor overnight in a sealed container at 80−100 °C. These silicas maintained their hydrophobicity even in a 60% methanol−water mixture. Nitrogen sorption measurements also indicated that the hydrophobicity treatments cause no pore size and size distribution changes in these aerogels. Figure 11 gives the overall process of producing hydrophobic silica aerogel

Table 6. Chemical Changes Occurring in the Aerogel Structure during Hydrophobization and Related Weight Losses upon Heating

gel structure	treatment[a]	T < 150 °C[b]	150 °C < T < 300 °C[c]	300 °C < T < 500 °C[d]
$Si_nO_{2n-(x+y)/2}(OR)_x(OH)_y$	gel I (as is)	1.7	8.2	1.0
$Si_nO_{2n-y/2}(OH)_y$	gel II (H_2O treated)	4.5	0.0	1.8
hydrophobized gel I				
$Si_nO_{2n-(x+z)/2}(OR)_x(CH_3)_z$	$(CH_3)_2(OCH_3)ClSi$	3.4	8.5	2.0
$Si_nO_{2n-(x+z)/2}(OR)_x(CH_3)_z$	$(CH_3)_3ClSi$	1.8	7.5	1.8
hydrophobized gel II				
$Si_nO_{2n-z/2}(CH_3)_z$	$(CH_3)_2(OCH_3)ClSi$	0.7	0.0	5.0
$Si_nO_{2n-z/2}(CH_3)_z$	$(CH_3)_3ClSi$	0.9	0.0	4.8

[a] Aerogels were exposed to the vapor at 100°c for 24 h in closed jars. [b] Differences in weight loss in this column are due to absorbed water. [c] Differences in weight loss in this column is largely due to alkoxy groups. [d] Differences in weight loss in this column are largely due to the hydrophobic alkyl groups.

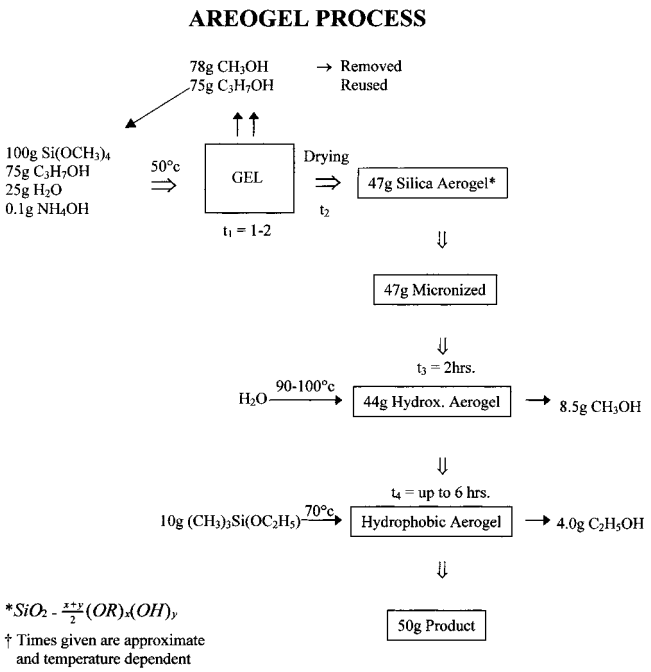

Figure 11. Process chart for producing hydrophobic silica aerogel powders with R value of 14, under non-supercritical conditions.

and aerogel powders optimized for thermal insulation under non-supercritical conditions.

A method by which gel formation and hydrophobizing occur concomitantly, in a single step, was later developed by using hexamethyldisilazane (HMDZ). The process (gelation and hydrophobizing) is autocatalytic, requiring no explicit catalyst addition and allows the use of tetraethyl orthosilicate (TEOS), as well as TMOS, as silica sources. It was discovered that there is a narrow window in the HMDZ/TEOS ratio that yields hydrophobic aerogels in ethanol that are remarkably similar to those currently produced from TMOS in 2-propanol. The process yields ~30% hydrophobic aerogels having 80% porosity. These aerogels can be further hydrophobized to the ~50% level by an additional exposure to HMDZ vapor. Perhaps one of the most important aspects of this process is that highly porous, hydrophobic aerogels can now be prepared using tetraethyl orthosilicate (TEOS) as the silica source. TEOS is a less expensive and less toxic silane than TMOS. We have discovered a narrow window in the HMDZ/TEOS ratio which yields hydrophobic aerogels in ethanol that are remarkably similar to those currently produced from TMOS in 2-propanol.

Table 7. Degree of Hydrophobicity Induced on Aerogel Powders as a Function of HMDZ Concentration in Aerogel Precursor TEOS−HMDZ Mix

HMDZ/TEOS		degree of hydrophobicity[a]
mol/mol	g/100 g	wt % methanol in H_2O
0.075	5.8	27
0.100	7.7	33
0.150	11.5	40
0.175	13.5	45
0.200	15.4	50

[a] Standard industry practice to measure the hydrophobicity as a function of methanol concentration in water, above which the powder starts to settle.

Hydrolysis reaction of HMDZ with water is found to be complete within 30 min at room temperature. NMR investigations showed that the hydrolysis product contains up to 90% active trimethylhydroxysilane monomers:

$$(CH_3)_3SiNHSi(CH_3)_3 + 3H_2O \rightarrow 2(CH_3)_3SiOH + NH_4OH \quad (17)$$

These monomers were stable at least 30 days as indicated by the NMR test conduced after 30 days. $(CH_3)_3SiOH$ species when mixed with silicon alkoxides can react both hydroxyl and alkoxy groups during the hydrolytic polycondensation of the aerogel structure, creating surfaces terminated by hydrophobic $Si-CH_3$ groups.

Table 7 summarizes the degree of the hydrophobicity produced as a function of HMDZ concentration in silica aerogels formed from TEOS in ethanol.

In summary, this new method not only eliminates all extra steps involved in the hydrophobitizing of aerogels but also makes the formation of hydrophobic aerogels from TEOS possible, leaving ethanol as the only byproduct. Details of this investigation will be presented in another paper.

4. Conclusions

An investigation was carried out to produce silica aerogels under non-supercritical conditions for thermal insulation. In this investigation hydrolytic polycondensation parameters that determine the porosity and pore morphology of the gel structure were first identified and then optimized by computer-designed experiments for minimum thermal conductivity. It was found that the optimum reaction mixture composition by weight is 20% $Si(OCH_3)_4$, 75% C_3H_7OH, 5% H_2O, trace NH_4OH. It has also been found that when hydrolytic polycondensation

of silicon alkoxides, including silicon tetraethoxide $Si(OC_2H_5)_4$, is carried out in combination with hexamethyldisilazane under certain conditions, the resultant aerogel is hydrophobic. Even though the tendency to fracture in this system is minimized, the gel nevertheless fractures into 2−5 cm size pieces during the drying, making it useless to be used as large panels for thermal insulation. However, micronized powder of this aerogel (3−10 μm size particles) exhibits thermal insulation characteristics which are twice that of precipitated silicas with similar porosity, when used in evacuated pouches, e.g., $R = 85$ vs $R = 40$. This is due to the remarkably low solid conductivity of the internal structure where the solid contacts are limited to point contacts. The addition of aerogel powders, even at <1 wt % loading, into paint and polyurethane foam has a significant effect on the overall thermal conductivity of such composite material systems.

A significant finding of this investigation is that the aerogels of this type, and presumably other gel systems, can be rendered to micronized fine powder form in situ without affecting their pore morphology, by gelling the system under vigorous agitation. In these cases, the particle size is determined by the fluid dynamics and shear force under which the gelation occurs.

Acknowledgment. The authors are grateful to Amanda Mottorn for her valuable assistance and contribution in the preparation of this manuscript.

CM9903428